Chapter 6

Nitrogen Ion Microscopy

Marek E. Schmidt, Masashi Akabori and Hiroshi Mizuta

Additional information is available at the end of the chapter

http://dx.doi.org/10.5772/intechopen.76383

Abstract

The gas field ion source (GFIS) can be used to generate beams of helium, neon, hydrogen, and nitrogen ions, among others. Due to the low energy spread and the atomically small virtual source size, highly focused ion beams (FIB) can be obtained. We discuss the history of the GFIS and explain the field ionization and field evaporation process in general. Then, the unique properties of the nitrogen ionization, originating from the molecular nature, are explained. We show how the nitrogen ion microscopy (N2IM) can be used to image and pattern samples. The unique contrast observed in samples with graphene or carbon is reported. Finally, we conclude with an outlook of the technology and possible key applications such as spatially localized nitrogen-vacancy center implantation.

Keywords: gas field ion source, N2IM, GFIS-FIB, secondary electron

1. Introduction

The development of scanning probe microscopy was driven by the challenge articulated by Richard Feynman [1], namely that it should be possible to write (and read) the *Encyclopedia Britannica* on the head of a pin. By using a focused electron beam to pattern advanced resist materials and later transfer them into solid matter by various processes, this challenge has been overcome. By improving the electron beam, it also became possible to image sub-10-nm-scaled structures in the scanning electron microscope (SEM, relying on the secondary electron generation) or the transmission electron microscope (TEM). The latter technique makes it possible to image individual atoms; however, it is restricted to thin samples. Encouraged by the nanometer scale resolution of the SEM, the replacement of electrons with ions was researched. Since energetic ions generate secondary electrons when interacting with matter, the focused ion beam (FIB) can be used for imaging as well. Due to the lack of other available

ion sources, the first one to gain widespread adaptation was the gallium liquid metal ion source (LMIS), which relies on the formation of the so-called *Taylor* cone. In addition, since ions are significantly slower than electrons for a given energy and their charge-to-mass ratio is smaller, the magnetic lenses in the SEM are replaced by electrostatic lenses. While a sub-5-nm beam diameter for gallium is possible today, the imaging resolution is limited to a few nm due to the immediate surface sputtering by the energetic ion impacts and the requirement to collect sufficient number of secondary electrons [2].

Energetic ions are used in other technological fields as well, such as ion implantation and surface etching (ion milling). These methods can be locally restricted by integrating with a mask; however, this requires several additional process steps, including a lithographic mask, and has limited resolution. Furthermore, this approach has a large initial cost. Instead, FIB can be used to locally mill structures at the nanometer scale with great flexibility. Important parameters are the etch rate and selectivity (difference of etch rate between two different materials for the same milling conditions), which can be improved by the so-called gas-assisted etching. For this purpose, thin needles are introduced close to the beam-sample interaction region, and minute amounts of gas are introduced. While the gas concentration is high at the point of injection, it is quickly evacuated by the pump system of the low-pressure sample chamber. By introducing special volatile precursor gases that are disassociated by the ion beam, the deposition of conducting as well as insulating materials is possible.

Gallium FIB is now widely used for rapid prototyping, circuit editing, lithographic mask repair, and TEM lamella preparation. However, several limitations have become more pressing in recent years:

1. The low milling resolution of the gallium ion (due to the large interaction volume of the heavy ions) is not sufficient for sub-10-nm fabrication, and the repair of next-generation optical masks becomes challenging. Furthermore, reflective UV masks have a higher requirement for defect-free repair.

2. The implanted gallium atoms can degrade the properties of the specimen. This is particularly critical for the preparation of TEM lamellae of certain samples and circuit editing where the semiconducting properties of transistors can change.

3. To improve the resolution of the gallium FIB, very low beam currents in the single-digit pA range are used. At these currents, the low secondary electron yield makes it difficult to do end-point detection, that is, notice when a given layer is fully removed.

In consequence, through meticulous ingenuity, the gas field ion source (GFIS) was commercialized. Initially, work focused on the ionization of helium ions as its ionization field strength clearly distinguishes it from other gases, and the light ions promise a superior imaging resolution while limiting the sample damage. However, today, there is a wide range of gases used, including helium, neon, hydrogen, and nitrogen. We discuss the GFIS in general in Section 2, and focus more on the uniqueness of the nitrogen field ionization in Section 3. In Section 4, we show how the nitrogen ion microscopy (N2IM)[1] can be used for imaging and patterning. Due

[1]The acronym *NIM* is now widely used to refer to the neon ion microscopy.

to the limited space, not all aspects can be discussed in full detail. As there is much overlap with the helium ion microscope, the excellent book edited by Hlawacek and Gölzhäuser [3] should provide answers to outstanding questions.

2. The gas field ion source

The GFIS, as the name suggests, is a type of ion source that works by ionizing gas atoms or molecules in a strong electric field. In this section, first, a short history of the GFIS is given for the interested mind, followed by the fundamental principle of the field ionization and field evaporation in strong electric fields. This also includes the discussion of the fundamental limits. In Section 2.3, the more technical aspects of exploiting the field evaporation and gas etching in order to make a good ion source are discussed. We also summarize some recent ion source developments beyond the GFIS that have been fuelled by the commercial success of the GFIS.

2.1. History of the gas field ion source

The foundation of the GFIS was laid by Müller [4], when he developed the field ion microscope (FIM). In a FIM, individual surface atoms of a metal tip can be imaged with relatively simple methods by applying a strong electrical field in a gas atmosphere. The gas atoms (typically helium) are ionized and are then accelerated away from the metal surface (**Figure 1a**). By allowing these accelerated ions to pass through a hole in the so-called *extraction electrode*, they can be visualized on a detector screen, as shown in **Figure 1b**. As the electric field at protruding atoms is stronger, ionization from these locations is more likely. This setup has to be located in a vacuum chamber to avoid high-voltage breakdown (arcing), and the emitting metal is typically cooled to increase the ionization rate. It quickly became clear that the emission from a single atom could, in principle, facilitate an ion source [5, 6] with unprecedented resolution (as will be discussed in Section 2.3); however, current stability turned out to be a serious issue [7]. In the meantime, the gallium LMIS was developed and offered sufficient performance for the time: a wide range of beam currents from the pA to the nA range, and sufficient resolution to allow prototyping and circuit editing in the semiconductor industry.

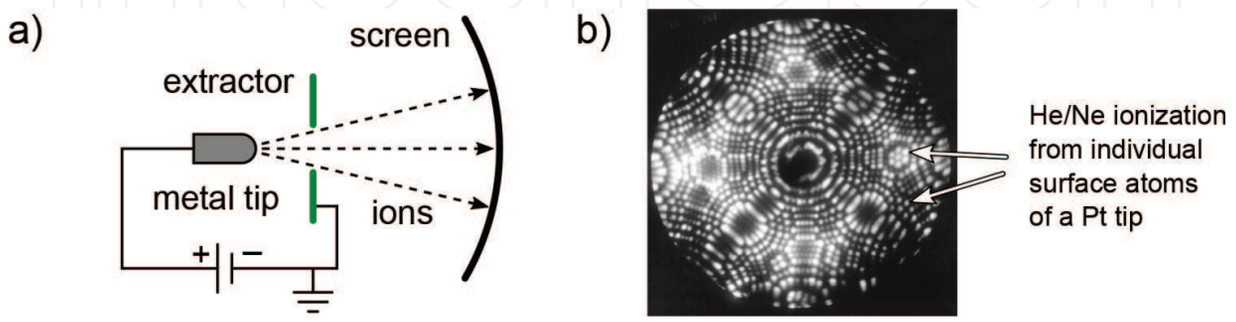

Figure 1. (a) Operation principle of the field ion microscope. (b) FIM image of pt tip (derivative of *platinum* (https://www.flickr.com/photos/dxdt22/315745462) by Tatsuo Iwata licensed under CC BY 2.0).

The development of methods to controllably shape noble metal tips through electrochemical etching, field-assisted evaporation, and etching remained active due to the demand for electron emitters.[2] The effort up until 2005 to develop high brightness, monochromatic noble gas ion sources was reviewed by Tondare [8]. It is now known that sometime in the 1990s, the active development of a GFIS commenced at the *Micrion Corporation*. The goal was to create a next-generation ion source to allow repair of photolithographic masks in the semiconductor industry, and the work was encouraged by the technological advances and the better understanding of the field emission [9]. However, after the first performance values were obtained and the theory had been reexamined, it became clear that in spite of being a source with unprecedented brightness, the overall emission current would not be on par with existing ion sources. The merit of this challenging technology became questionable, and furthermore, the development team was haunted by stability issues of the novel source. Nevertheless, the development team succeeded in forming a GFIS emitter from Tungsten that was terminated by three atoms aligned in a triangle, the so-called *trimer*. The trimer can improve the stability compared to a single atom tip for certain tip materials and crystal orientations; however, only one-third of the total brightness is usable. First results demonstrated that the GFIS would be an ideal candidate for an ion microscope that could excel the SEM with a sub-1-nm beam diameter and favorable beam/sample interaction. However, commercialization was not yet viable.

With this result, Bill Ward continued the improvement of the source stability—the last remaining obstacle before commercialization—after parting with *Micrion* upon their acquisition by the *field electron and ion company* (FEI). After 2 more years of ups and downs, and just as the team had moved to a new location, a demonstration was to be given to potential investors. To the surprise of Ward himself, the stability and performance was significantly better than just before the move. As it later turned out, due to time constraints, a special custom-made gas purifier was not installed to the gas supply in the new location. At some unknown point in the past, a piece of wooden cork had slipped into the tube of the purifier and got stuck. Thus, the gas supplied to the ion source had been passing through the cork during the development time, and this was the root cause for the low stability. However, as Ward recalled during his speech at the 2016 AVS International Symposium & Exhibition in Nashville, Tennessee, commemorating the 10th anniversary of the commercialization of the GFIS [10], during the struggle with the stability of the GFIS, the team gained experience and knowledge that turned out to be indispensable to the commercialization. Would it not have been for the long development time and investment to overcome the instability before realizing the current limitation, the effort to commercialize the GFIS would have likely been dropped earlier in the development.

With investors on board, the Atomic Level Ion Source (ALIS) company went public with its results in 2006 [11, 12]. Shortly after, *ALIS* was acquired by *Carl Zeiss'* Nano Technology Systems Division (NTS), and the *Zeiss Orion* helium ion microscope was the first commercial GFIS tool released in the same year. Development in the time since then progressed; however, the fundamental GFIS technology remains the same, and new tools are now fitted with helium

[2]Technically, the difference between a GFIS and a field emitter gun for electrons is the polarity of the tip with respect to the extractor electrode. Since electrons are supplied through the tip, cooling is not required for electron emission.

and neon gas. The events surrounding the development of the HIM at *Micrion* and *ALIS* were also recollected by Economou et al. [13] and Ward himself ([3], Appendix A).

The impressive results achieved by the *Zeiss Orion* certainly renewed the interest in GFIS, and the Japanese gallium FIB specialist *SII Nanotechnology* presented results on their hydrogen and nitrogen GFIS-FIB nanofabrication tool for the first time in 2011. Unprecedented mask repair performance, particularly of reflective UV masks, was reported [14]. Shortly after, at the beginning of 2013, *SII Nanotechnology* was acquired by *Hitachi High-Technologies* and continues operating under the name *Hitachi High-Tech Science*. *Zeiss* and *Hitachi* appear to remain the only commercial manufacturer of GFIS tools. Nevertheless, it is likely that sooner or later other players will enter the field of light gas ion FIB technology. As we show in Section 2.4, this does not have to be necessarily a GFIS.

2.2. Field ionization and field evaporation

To understand the field ionization (gas atoms losing an electron in a strong electric field) and field evaporation (surface atoms detaching due to high electric field), some general knowledge about solid state physics is required. The GFIS is used by scientists and engineers from a broad range of fields, and for the daily use the details that will be explained in this section are not necessary. Nevertheless, it is helpful to understand the potential and limitation of this technology. Therefore, we give an explanation in a way that can be followed by readers from various fields, and details can be found in the excellent books that have been written over the years [15–18].

In solid state physics, there are a few concepts which are prerequisites in this discussion:

1. **Energy versus position** is a common representation of the inner properties of solids as seen by electrons. The position is typically a one-dimensional line through the solid as it contains the essence of the solid and can still be easily interpreted. Two-dimensional (2D) or even three-dimensional (3D) representations exist, but are less common. The energy (sometimes called potential, *y*-scale) is given in units of electron volt (eV) and defines *relative* energies, that is, there is no zero point as it is irrelevant.
2. **Fermi energy** (E_F) is the highest energy an electron in a given material can have at absolute zero Kelvin. At elevated temperature, some electrons from below E_F are *excited* and gain some additional energy.
3. **Vacuum energy** (E_{vacuum}) is defined as the energy outside of the solid in vacuum.
4. **Work function** is an energy difference that is unique to each individual electron in a solid. It is the energy that has to be added to the electron's energy to make it reach E_{vacuum}, thus separating it from the solid.
5. **Quantum tunneling** is a phenomenon where electrons can cross a potential barrier although they do not have enough energy to reach the top of the barrier (given that the space behind the barrier is unoccupied). Electron energy is conserved. The tunneling probability increases rapidly with the decrease of the barrier width, and the Pauli principle

forbids tunneling into energies below E_F. This phenomenon does not occur in the visible world. A possible image of quantum tunneling could be as follows: Let us imagine a golf ball lying in the grass next to a solid concrete wall. Tunneling would mean that there is a chance that the ball moves to the other side of the wall without being touched.

Figure 2a shows a 2D cut through a large metal, where the atoms are assembled in a regular structure. If we plot the energies along the red line, we obtain **Figure 2b**. Here, + represents the positively charged cores of the individual atoms. They create *energy wells* for electrons through their Coulomb potential, which are filled with some electrons of specific (*quantized*) energy. Since the energy of these electrons is considerably smaller than the top of the barrier between

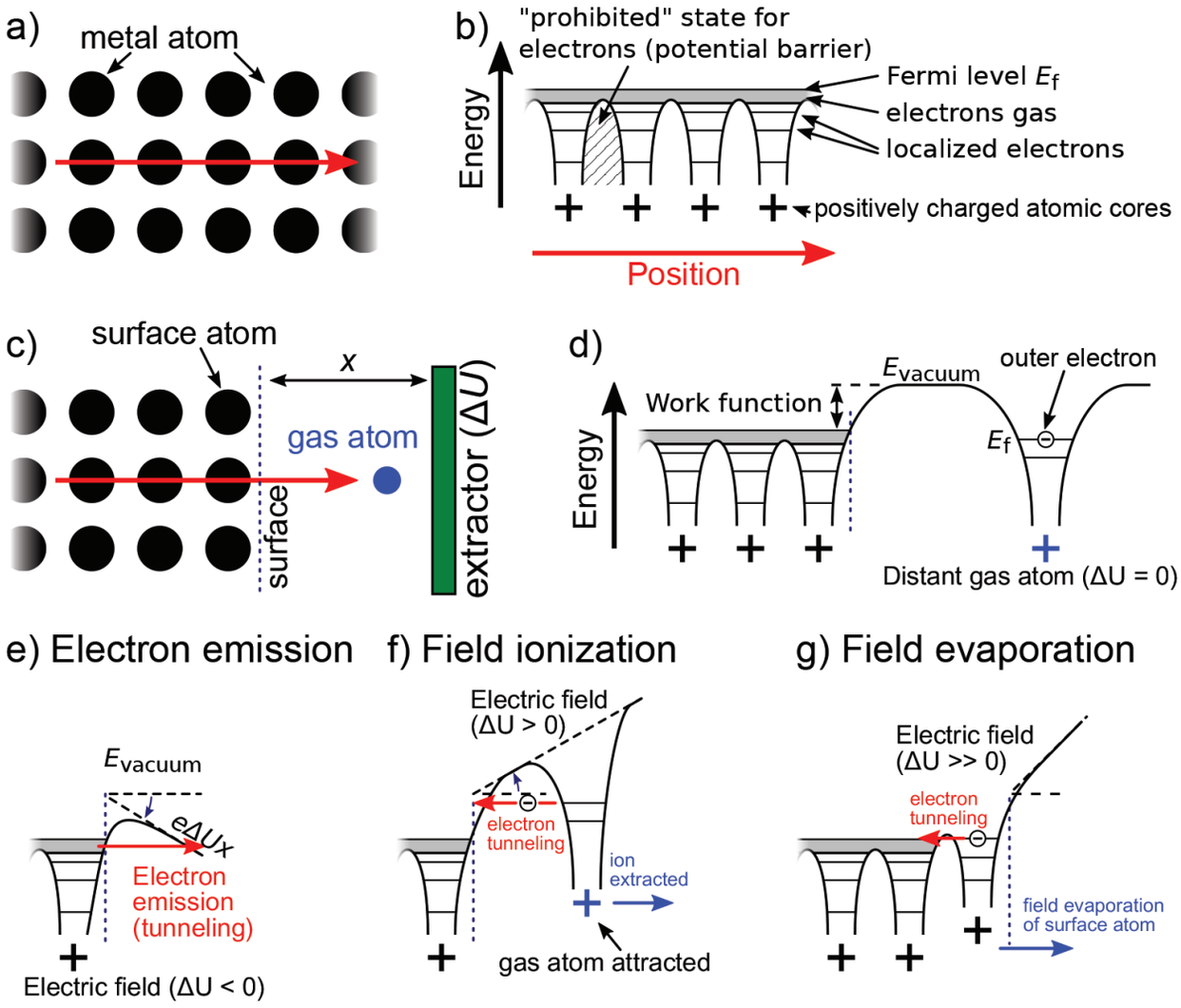

Figure 2. (a) Model of metal atoms inside a bulk metal. The potential along the red arrow is shown in (b). (b) Potential inside bulk metal. Electrons are either localized near the atoms or can move freely if they have sufficient energy. These electrons are referred to as *electron gas* and give metal the high electrical conductivity. (c) Model of metal surface with an extractor electrode at distance x and a gas atom. (d) Potential along red arrow in (c). (e) Narrow potential barrier formed by negative ΔU resulting in electron emission. (f) Positive ΔU causes electron tunneling of outer electron of nearby gas atoms. The ion is immediately accelerated toward the extractor. (g) Further increase of ΔU causes field evaporation of surface atoms.

the atoms, they are assumed to be *localized* and do not contribute to electrical conduction. However, since E_F is higher than the barriers (this is only true for metals), there are some electrons that can move freely from left to right. They are part of the so-called *electron gas* which gives metal its high conductivity. Since the metal is periodic, this energy profile is periodic as well.

As pointed out at the beginning of this section, field ionization occurs only at the surface. Therefore, let us see what happens when we cut our metal to create a surface as illustrated in **Figure 2c**. We ignore the extractor for now ($\Delta U = 0$), and observe the energy profile along the red arrow as shown in **Figure 2d**. To the left of the surface, the potentials are unchanged; however, at the surface, a potential barrier reaching up to E_{vacuum} is formed. Thus, the electrons in the electron gas are reflected at the surface and remain inside the metal. Furthermore, a gas atom that is far away from the surface creates its own potential well, and all its electrons are localized. Note that the electron with the highest energy is referred to as the *outer* electron. If we were to observe the gas atom and surface at this condition, we would see that the gas atom moves randomly in respect to the metal surface, but no ionization occurs. Also, since the energy of the outer electron of the gas atom is below E_F of the metal, the electron cannot tunnel to the metal, even if the barrier width was greatly reduced due to collision with the metal surface (Pauli principle). The system is stable.

To actually cause anything to happen, an electric field has to be applied between the metal surface and the extractor electrode. Again, let us first ignore the gas molecule and discuss the electron emission. If we apply a large positive voltage to the extractor (at a distance x) while the tip is grounded,[3] the potential barrier at the surface is deformed as shown in **Figure 2e** and electrons can tunnel from the metal into the vacuum. The slope equals $e\Delta U x$, where e is the electron charge. As the density of electrons in the metal is high and a virtually infinite supply is available, very high emission currents can occur, and Joule heating of the metal poses the limit.

However, since we are trying to ionize gas, let us go back to the configuration shown in **Figure 2d** and apply a positive ΔU instead (**Figure 2f**). Two things are now happening: first, the vacuum energy increases away from the surface, and second, the energy of the outer electron of the gas atom becomes higher than E_F of the metal. Gas atoms have fluctuating dipole moments as the outer electrons are orbiting around the core, and this causes the gas molecule to be attracted to the metal surface in the strong field. In consequence, all prerequisites for tunneling of the outer electron of the gas atom are fulfilled: the barrier is narrow, and there is space for the electron in the metal at the energy of the outer electron. After tunneling, the now positively charged gas *ion* is immediately accelerated in the strong electric field away from the tip and toward the extractor. The ion has an energy corresponding to ΔU. For the ionization to happen, the field has to be in the range of 10^{10} V/m. For a flat surface, this would correspond to 100 MV at $x = 1$ mm. However, by using a sharp needle instead of a flat surface, the electric field is concentrated at the tip apex, and only 5 kV is required for a tip diameter of

[3] We can also apply a negative voltage to the tip and ground the extractor. Important is the potential difference ΔU. Note that lower potential corresponds to a higher energy. This counter-intuitive definition is of historic origin.

100 nm. Some individual surface atoms that stick out due to the crystal structure cause a localized concentration of the field, and ionization occurs predominantly there (see **Figure 1b**).

By further increasing the electric field, the attractive force of the gas atom is stronger, resulting in a higher tunneling probability (which can be estimated by the *Wentzel-Kramers-Brillouin* approximation). This is directly reflected in a higher ion current. However, an exceedingly large field will cause field evaporation (**Figure 2g**). The potential of the surface metal atom is slightly increased, and one of the localized electrons can tunnel into the bulk. The temporary positive charge of the surface atom can be enough to break it away in the strong electric field. For field ionization, we can therefore conclude that we require enough electric field to attract the gas atom and allow tunneling; however, the evaporation field strength should not be reached. The actual voltage that has to be applied to the extractor depends strongly on the distance x and the shape of the tip. Furthermore, different gases require different field strengths for ionization, with helium being the highest at 4.4×10^{10} V/m [19]. This poses a technological challenge for the control of the ion beam energy: by grounding the extractor electrode and varying the tip potential, the kinetic energy of the ions after passing through the hole in the extractor can be vastly different. This is solved similar to the LMIS and FEG with the introduction of an accelerator electrode that allows extraction control independent of the final beam energy (see **Figure 3a**). The ion column of the GFIS-FIB nanofabrication tool located at the *Japan Advanced Institute of Science and Technology* is illustrated in **Figure 3b**. The microchannel plate that can be inserted into the ion beam is used to image the emission tip in the FIM mode.

2.3. The emitter tip

As discussed in the previous section, to reduce the requirement on the voltage that has to be applied to the extractor, a sharp tip is used. However, this is not the only reason. In the GFIS, the limit of current (i.e., the rate of ionization events) is mostly limited by the supply of the gas atoms. In fact, the main route of gas supply is through the attraction of gas atoms to the shaft of the tip where the electric field is weaker, followed by migration or hopping toward the apex. Thermal vibration of the tip can repel some of the adsorbed gas atoms and constitutes source vibration, thus the cryogenic cooling mentioned earlier. The ionization rate can be directly controlled by the pressure of source gas around the tip; however, exceeding a certain limit might cause arcing between highly charged parts, which has to be avoided. Also, atom-atom collisions reduce the mean free path. It should thus be clear that if a tip has several ionization sites close to each other, they compete with each other for the available gas.

The achievable diameter of a focused ion beam, D, is given by [21].

$$D = 2R = 2\sqrt{(MR_S)^2 + \left(\frac{1}{4}C_{si}\alpha_i^3\right)^2 + \left(\frac{1}{2}C_{ci}\alpha_i\frac{\Delta E}{E}\right)^2}, \quad (1)$$

where R is the beam radius, M the magnification of the optics between the source and the sample (between 0.3 and 2), R_S the source size, α_i the beam cone angle, C_{si} and C_{ci} the spherical and chromatic aberration coefficients, respectively, and E the acceleration voltage. ΔE is the

http://dx.doi.org/10.5772/intechopen.76383

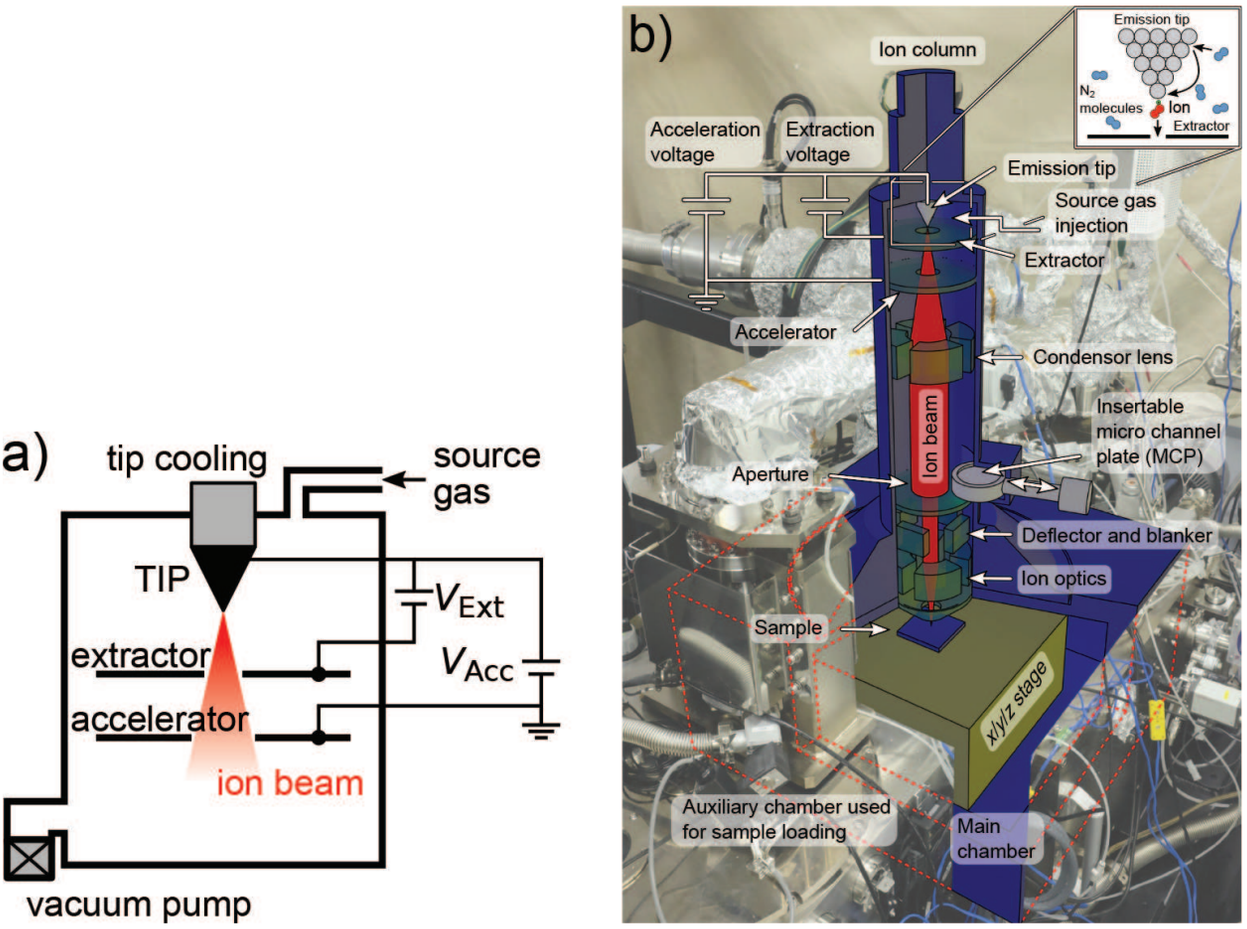

Figure 3. (a) Configuration of emission tip, extractor, and accelerator electrode in the GFIS. (b) Schematic illustration of the ion column of the GFIS-FIB nanofabrication tool. The field ionization process is illustrated in the inset. Reproduced with permission [20].

energy spread, which is the variation of energy of individual ions. To minimize D and thus have the highest resolution, the atomically small R_S and the low ΔE of less than 1 eV [11] are unique to the GFIS and surpass other ion sources. The beam diameter estimation in Eq. (1) assumes that only the emission from a single emission site is aligned with the microscope column, and the emission from the remaining ionization sites is either lost in the ion optics or filtered by a narrow aperture. There had been considerations to focus emission from multiple sites; however, this has proven to be technically not feasible. For the HIM with the tungsten tip, the *trimer* is a compromise between stability (i.e., the three atoms of the pyramid stabilize each other) and brightness of $\sim 4 \times 10^9$ A/cm^{2}sr which can be achieved [12]. In other cases, a single atom tip (SAT) can be formed [22, 23], which can improve source brightness especially for heavier gas atoms that are not as mobile as helium, and the total supply of gas atoms is the limiting factor.

The formation of good emitter tips requires a high level of specialization. Starting from a thin wire of pure metal with as few crystal defects as possible, electrochemical etching [24] is used to form the nanoscopic shape. Then, while observing the emission in an FIM, field evaporation, gas-assisted etching (surface atoms at the shaft of the tip are removed in oxygen or nitrogen

gas atmosphere at fields above the individual ionization field strengths [25]), and emitter heating (causing migration of surface atoms) are used to form the atomistic tip structure. The latter processes can be performed in situ once the emitter is fitted in a microscope, as well. As the ion emission originates from the tip apex and follows the electric field lines, the positioning requirement of the emitter tip in respect to the ion column is unproblematic.

Recently, it has been demonstrated that a tungsten tip can be coated by a thin layer of iridium [26]. Due to the softness of tungsten, it can be shaped more easily, while the extremely sturdy iridium can improve emission stability.

2.4. Other novel ion sources

The renaissance of the FIB with the significantly improved performance of the GFIS compared to the LMIS, as well as the prospect of a large ion portfolio, has led to intensive research into other ion sources as well. For example, gas atoms can be trapped and cooled in the magneto-optical trap (MOT). After condensing them, another light source is used for photoionization, and the ions are extracted in an electrical field [27]. The gas trapping can also be achieved by laser cooling alone [28]. Although the range of possible gases to be ionized by this method is unlimited, the wavelength of the cooling and ionization lasers has to be adjusted for each species which adds to the cost of the source.

3. The nitrogen ion beam

Nitrogen is unique compared to other source gases used in GFIS, as it forms one of the strongest bonds known in nature (binding energy: 9.79 eV; bond length: 0.11 nm) and naturally occurs only as N_2. Nitrogen can be ionized by electron impact, and the effect of nitrogen ion impact on various materials has been investigated [29]. By annealing exposed silicon samples, the formation of Si_3N_4 was reported [30, 31]. The measurement of electron impact ionized nitrogen mass spectra revealed that while N_2^+ ions dominated, some N^+ ions are generated as well [32]. Since the resolution of ion beams in accelerators is in general no issue, a mass filter is typically added to the beam line that removes unwanted ions and leaves a pure beam of required ions. For the GFIS, where we strive for highest resolution, a mass filter would degrade the beam and the ion beam should be pure "as is," Otherwise, two beams are scanned across the sample with a separation depending on the mass difference and the magnetic field occurring along the ion's path. In this regard, N_2 has the advantage of naturally high isotopic purity.

In Section 3.1, we explain what happens during field ionization of nitrogen and interaction with a silicon sample. Then, the nitrogen GFIS-FIB is compared with other ion species used in the GFIS in Section 3.2.

3.1. Field ionization of molecular nitrogen gas and solid-ion interaction

The possible ionization mechanisms of N_2 gas and how they behave after impact on a solid silicon sample are shown in **Figure 4**. In addition, Monte Carlo (MC) simulation results for

http://dx.doi.org/10.5772/intechopen.76383

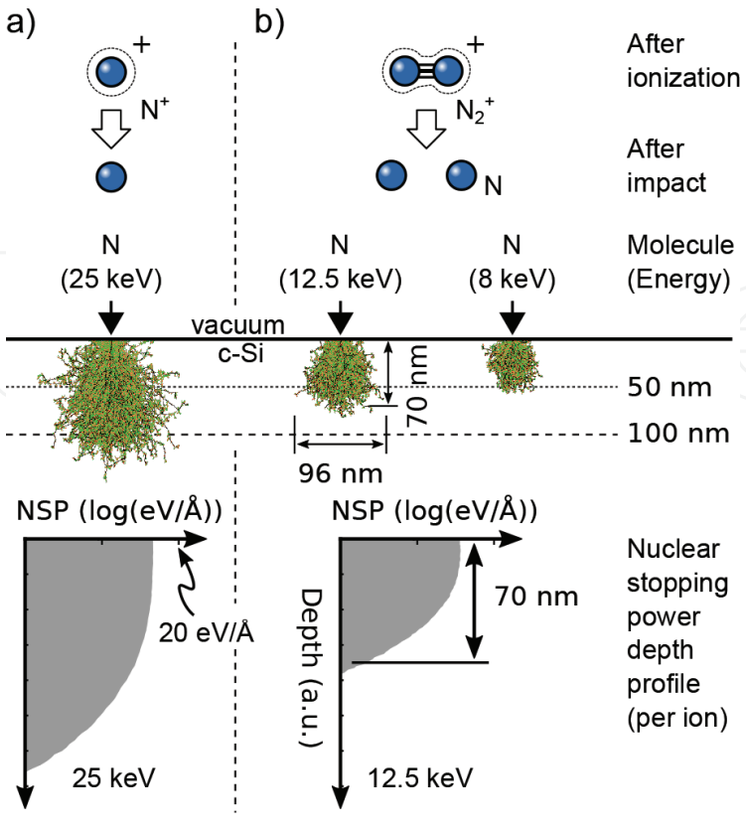

Figure 4. Possible ionization mechanisms of N_2 gas ionized in a GFIS [32, 33] together with MC simulation results for 25-kV acceleration voltage: (a) The molecule splits during ionization and interacts with the sample as an atomic ion with full energy and (b) the molecule stays together during ionization but splits upon impact (modeled as N with 1/2 energy). The interaction volume and nuclear-stopping power depth profiles for the two cases show the different sizes of the expected damage region. In addition, the interaction volume for 16-kV acceleration voltage is shown (modeled as N with 8 keV). Reprinted with permission [39]. Copyright 2017, American Vacuum Society.

these two possibilities with an acceleration voltage of 25 kV are shown. Collision cascades (i.e., the way atoms proceed through a solid after collision) are very difficult to simulate.

The most accurate method is the so-called molecular dynamics (MD) approach, where each individual atom is modeled, and the forces acting onto each other are evaluated accurately. With each additional atom in the simulation model, the complexity increases exponentially, and it is not realistic to simulate a system with several thousand atoms—the number of atoms in the range of the ion—due to the computational cost. Furthermore, the result would be vastly different depending on whether the ion directly collides with a surface atom (possibly resulting in backscattering) or channels along crystallographic directions. Thus, to obtain a complete understanding of the possible effect of the ion beam, a large number of MD simulations would be required where the position and angle in respect to the target crystal are varied. This approach is only viable in special cases, as demonstrated in a study of ion interaction with an atomically thin membrane [35]. MC takes a different approach, which uses probability to simplify complex processes. If an ion is traveling through a medium, it is easy to understand that it has a chance to collide with atom cores or pass between atoms. Instead of explicitly calculating the outcome, a probability of collision is considered that depends on the projectile and the density and composition of the target sample. Furthermore, the possible outcome of

collisions (i.e., the amount of energy lost and the change of direction) can also be assigned to probabilities. Now, to actually perform the MC simulation, a particle with a given direction and velocity is assumed. Based on these parameters, the position of the particle after a certain time τ is calculated. Furthermore, the occurrence and type of interaction is calculated for this time step with the help of the previously mentioned probabilities and a random number generator. With this, we can define a new direction and velocity (which can be unchanged or point to the side) and calculate the position after the next time step. This process is repeated until the particle either left the medium or its velocity dropped below a threshold. Since this result might be far away from the reality as it relies on the random number generator, the outcome of particles with the same initial conditions is repeated for several thousand times, each time with a different outcome. By plotting all the trajectories and evaluating the recorded collision details, the principle shape of the interaction region as well as the mean range can be estimated with small computational cost. For example, we can see that for a N^+ ion at 25 keV (**Figure 4**), damage deeper than 100 nm from the surface will occur. Factors limiting the accuracy of the MC simulation method is the fact that each "shot" is performed onto a pristine target (i.e., no accumulation of damage), and it requires experimental data to model the particle-medium interaction as precisely as possible. SRIM is one software package for MC simulation that has proven useful for many cases [36], but other MC codes exist [37, 38].

To determine which of the two possible ionization mechanisms shown in **Figure 4** is the one that occurs in the GFIS, a crystalline silicon sample is exposed, and the cross section can be observed by TEM, as shown in **Figure 5**. Here, several exposures with different doses were performed with 25 keV and one additional one at 16 keV. As silicon changes from crystalline to amorphous above a well-defined disorder threshold, the observed shape in the TEM is a good indicator of the range of ions. By comparing the shape of the bell-like amorphous region with the MC simulation, it was thus possible to confirm that the N_2 molecules are ionized to N_2^+. As energetic ions are instantaneously neutralized upon impact onto a solid through the pickup of an electron, the impact of a N_2 molecule onto silicon was calculated by atomistic simulation as well [39]. It confirmed that the N-N bond is broken within a few atomic layer, and the N atoms

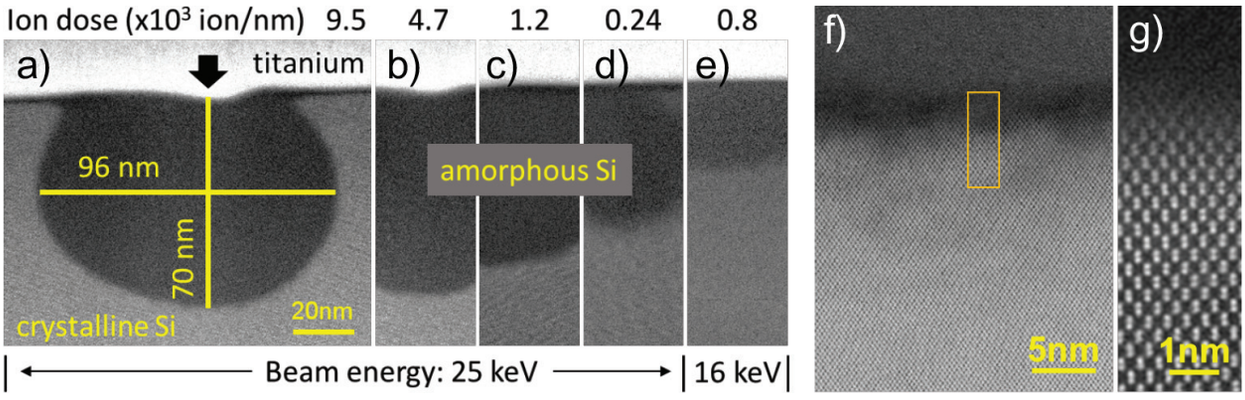

Figure 5. High-resolution HAADF-STEM micrographs of N_2^+ bombarded bulk crystalline Si for 25-keV beam energy at doses of (a) 9.5 to (d) 0.24 × 10^3 ions/nm, and (e) 16 keV at 0.8 × 10^3 ions/nm. Scale bar is the same for all images. (f) High-resolution ABF-STEM micrograph of the transition region from crystalline to amorphous Si for the implantation shown in (a). Although some amorphization is observed up to 10 nm away from the amorphous region, the well-defined transition is visible. (g) Atomic resolution HAADF-STEM image of the area indicated by the rectangle in (a), which shows the dumbbell structure of Si(110). Reprinted with permission [39]. Copyright 2017, American Vacuum Society.

http://dx.doi.org/10.5772/intechopen.76383

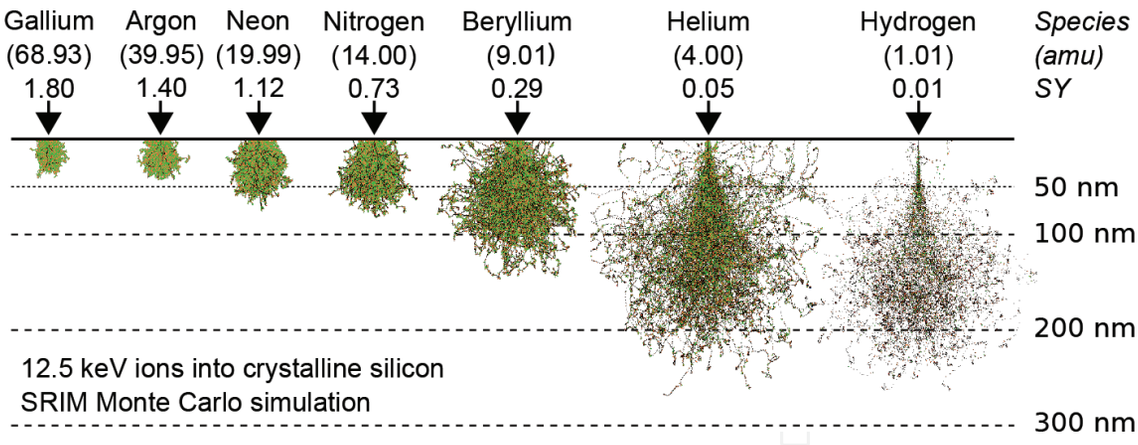

Figure 6. Comparison of interaction volume and sputter yield for Ga, Ar, Ne, N, Be, He, and H for corresponding ion energies of 12.5 keV. Reprinted with permission [34]. Copyright 2017, American Vacuum Society.

continue their path through the sample independently. Therefore, the ion beam with an acceleration voltage of 25 kV in the N_2 GFIS has the same effect on a sample as a N^+ beam with 12.5 keV would have.

3.2. Comparison with other ion species

Previously, various atomic ion species used or potentially usable for FIBs had been compared, based on MC simulation at 30 keV [40]. It impressively shows the advantage of light ions compared to heavier ions, namely the small interaction volume close to the surface, resulting in high milling and imaging resolution. To add nitrogen ions to this comparison, however, some care has to be taken. The MC simulations are based on atomic projectiles. Thus, when simulating the effect of the N_2^+ GFIS-FIB with an acceleration voltage of 25 kV, we have to perform a simulation of N with an acceleration voltage of 12.5 kV instead. If the N_2^+ GFIS-FIB was to be added to the comparison by Tan [40], the acceleration voltage of 60 kV would have to be assumed. This is outside the operation range of FIB microscopes. Therefore, in **Figure 6**, a comparison of different ions for a fixed energy (12.5 keV) is shown instead [39]. As expected from the different masses of the atoms, the penetration depth of nitrogen falls between beryllium and neon, with a sputter yield of 0.73 (i.e., the number of silicon atoms sputtered per impinging ion). It should be noted that this sputter yield considers a single N atom with 12.5 keV; however, the N_2^+ beam will actually yield two of such projectiles. To characterize ion exposure, the number of *primary* ions is typically reported. Thus, if we compare a certain dose of helium ions at 12.5 keV with N^+ at 12.5 keV (actually generated from a 25 keV N_2^+ beam), the nitrogen dose has to be doubled to predict the number of secondary electrons.

4. Nitrogen ion microscopy

Focused ion beams can be used for different types of microscopy. For example, back-scattered ions can reveal details about the atomic mass of target atoms (the imaged target atoms have to

be heavier than the ion species). In the secondary-ion mass spectrometry (SIMS), target atoms are sputtered and characterized in a mass spectrometer. Furthermore, ionoluminescence and transmission of ions through a thin probe can be used for analysis and imaging. However, we focus our discussion on the predominantly used secondary electron imaging due to the simplicity and the good perceptive sense of surface topography in images.

Light ions generate more secondary electrons compared to gallium ions [41]. Therefore, lower doses are sufficient to image a sample compared to gallium FIB, or for low doses visibility is better with light ions. The recent down-scaling of integrated circuits has increased the demand for milling at the single-nm scale, which can only be achieved by gallium FIB with extremely low beam currents. This results in the difficulty to do end-point detection and drives the interest in SE imaging by light ions. A large amount of HIM SE images can be found throughout the literature. The shorter wavelength of helium ions compared to electrons allows a smaller spot, and the small interaction volume at the surface means that the secondary electron generation is restricted to a smaller area on the sample. Regarding nitrogen, Schmidt et al. reported secondary electron images of samples imaged by helium and by nitrogen ions [20].

Secondary imaging is, even with an electron beam in the SEM, almost always a destructive method. Sample chambers in scanning probe microscopes have typical base pressures of $>1 \times 10^{-5}$ Pa due to the fact that rubber o-rings are used to seal some of the large openings that are required to install the sample stage. The ultra-high vacuum alternative is the usage of copper gaskets that, through compression between knife-edge flanges, create extremely good vacuum seals. This increases the cost of the chamber and machine maintenance. Alternatively, it is possible to achieve better vacuum by installing two rubber o-rings, where the space between the rings is evacuated by a separate pump. Such measures would further require ultra-high cleanliness of the images specimen and reduce the machine throughput. The contamination in the chamber is typically hydrocarbons that are emitted from the pump system, and as the beam (again, this applies to electron as well as ion beams) hits the sample, some of the adsorbed hydrocarbons are disassociated, and amorphous carbon is deposited on the sample. This carbon modifies the sample surface and can influence secondary electron emission. In addition, the charging of the sample occurs immediately. Other effects that influence SE emission are as follows:

1. work function,
2. charging (note that ion beams will always cause positive charge due to the implantation of positive ions and emission of electrons, while negative charging can occur in SEM),
3. escape depth of SE,
4. energy spectrum of SE.

Due to all these effects and the fact that imaging is "destructive," the prediction of SE yield remains impossible even for electrons. Therefore, while secondary electron yield (number of SEs emitted per incident particle) observed in a typical microscope might not be universal, they represent values "appropriate to the actual operational environment" [42]. Comparison of images has to be carefully discussed.

http://dx.doi.org/10.5772/intechopen.76383

4.1. Unique contrast in carbon-based samples

By imaging samples with carbon-based materials by focused nitrogen and helium ion beams, it was reported that an improved SE contrast is observed by nitrogen [20]. The sample that was imaged is shown in **Figure 7**, which comprises electrically contacted four-layer graphene and graphite on SiO_2 with gold electrodes. Particularly, it was noticed that the graphene, which is pulled-in onto the SiO_2 substrate, is only visible by N2IM. In addition, the authors confirmed that the observed contrast difference was not caused by equipment differences, and re-imaged the structures in the *Zeiss Orion Plus* [42].

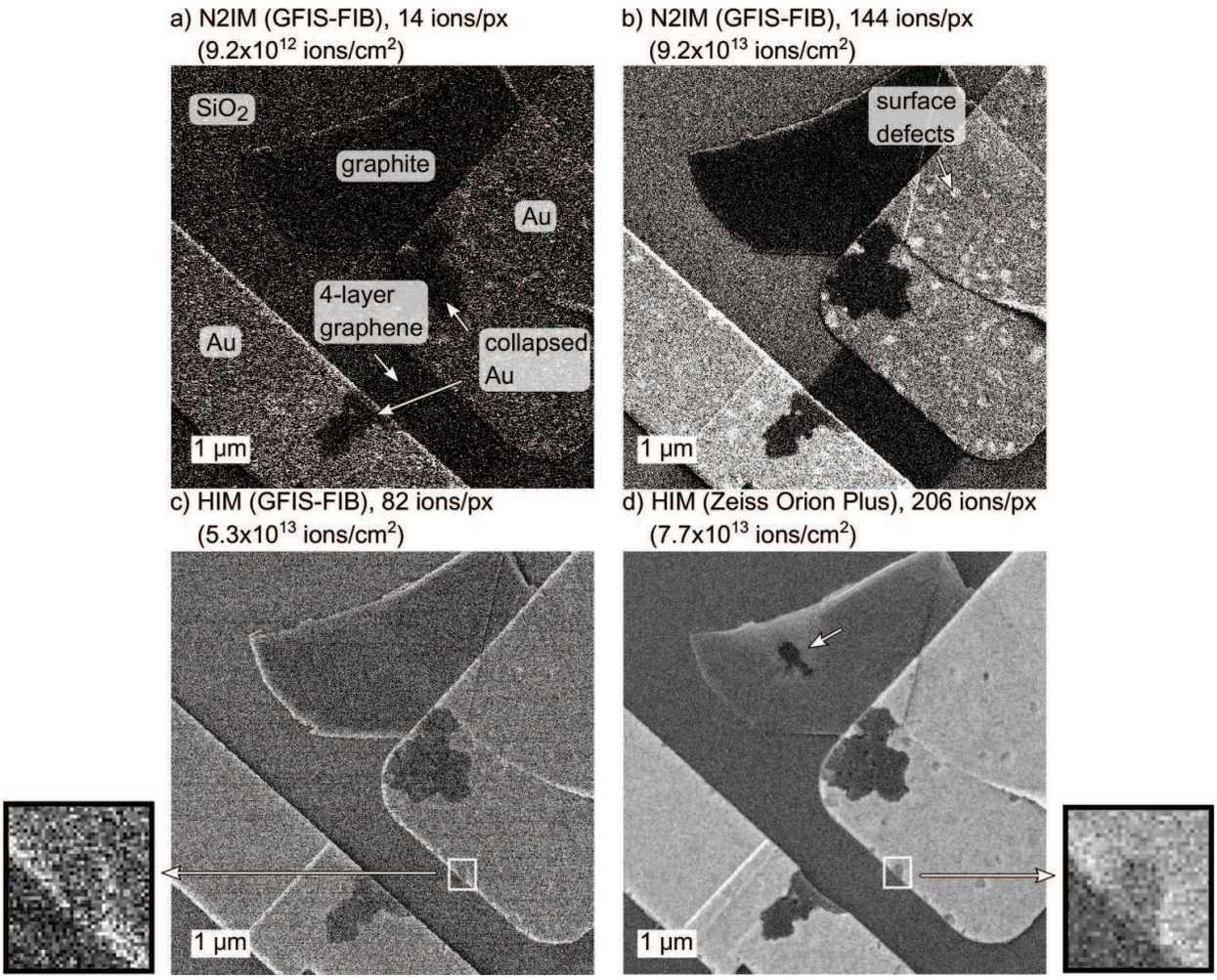

Figure 7. Secondary electron images acquired on identical location on nano-patterned sample. (a+b) N2IM (GFIS-FIB) images with 14 and 144 ions/px imaging dose at 25 keV. Graphite and four-layer graphene have good contrast against SiO_2 and Au electrodes. (c) HIM (GFIS-FIB) image with 82 ions/px at 25 keV. (d) HIM (Zeiss Orion Plus) image with 206 ions/px at 30 keV. The dark area in the graphite (arrow) is only visible in this image and probably formed after the previous imaging. Marek E. Schmidt, Shinichi Ogawa, Hiroshi Mizuta, "Contrast Differences Between Nitrogen and Helium Ion Induced Secondary Electron Images Beyond Instrument Effects," MRS Advances, DOI: 10.1557/adv.2018.33, reproduced with permission [42].

Interestingly, the thick graphite and the SiO_2 substrate had been exposed to a relatively strong oxygen reactive ion etching process, and the contrast difference was not observed for nanocrystalline graphene (NCG), a polycrystalline carbon film that can be deposited via a metal-free plasma-enhanced chemical vapor deposition at the wafer scale [43]. By imaging another sample comprising suspended graphene and electrically contacted graphite that was not exposed to the RIE (**Figure 8**), the contrast difference could be gradually induced by an accumulated nitrogen ion dose of more than 4×10^{14} ions/cm^2 [20]. Although the final cause for the contrast difference is not yet fully understood, it has thus become clear that the surface modification through the RIE process together with the nitrogen beam results in the observed effect. Strangely, however, the contrast difference appears to be temporary while observing with nitrogen. It should be interesting to see if adsorption of the reactive nitrogen atoms to the surface (nitrogen can be ejected from the sample surface, compare **Figure 6**) can cause a temporary change of work function and is removed shortly after imaging is stopped. Nevertheless, any added contrast can enable the imaging of samples that would otherwise remain unobservable. The effect of charging on the contrast is clearly visible in **Figure 8a**. Isolated gold and graphite gradually become darker as it is scanned by the nitrogen beam from top to bottom, while the contacted graphite retains its initial brightness.

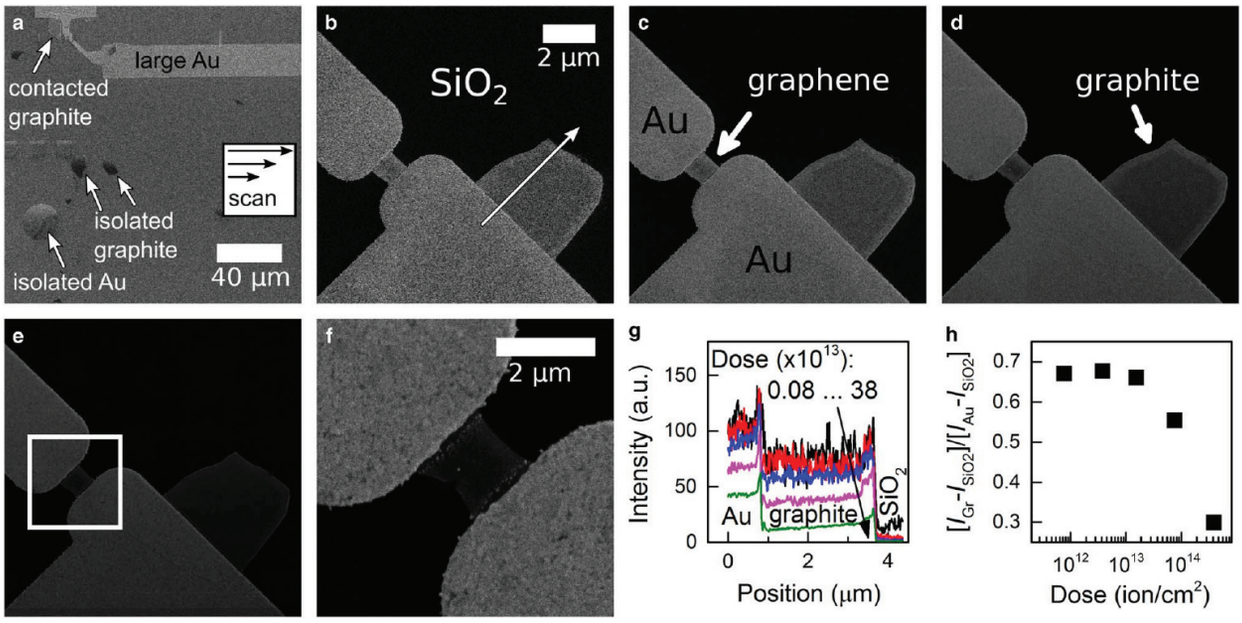

Figure 8. (a) Low-resolution N_2^+ GFIS-FIB image ($\sim 6 \times 10^{10}$ ion/cm^2) of sample C6 showing large Au electrodes with a contacted graphite flake, as well as isolated graphene and Au pattern. The isolated pattern shows decreased brightness from top to bottom caused by charging during the scan (scan direction illustrated in inset). (b–e) Series of images with a gradually increasing dwell time of identical location on sample C6 comprising suspended bilayer graphene and a larger graphite flake. The dose is increased from 6 ($\sim 3.8 \times 10^{12}$ ion/cm^2) to 24, 120, and 600 ion/cm^2. (f) A higher-resolution scan of area indicated by black square in (e) with 120 ion/px ($\sim 8.5 \times 10^{14}$ ion/cm^2). (g) Pixel brightness profile along the arrow shown in (b). (h) Relative graphite brightness as a function of accumulated dose extracted from (g) showing a decrease at high dose. Reproduced with permission [20].

http://dx.doi.org/10.5772/intechopen.76383

4.2. Nanomachining

Nanomachining of nanoscopic structures is one of the main advantages of the FIB over the SEM. At the beginning of this chapter, we discussed the motivation of the light gas ion source development, namely a higher milling resolution than the heavy gallium.

Helium has been demonstrated to offer unprecedented milling resolution of suspended layers [44] with a $\sim$ 5-nm wide graphene nanoribbon (GNR) realized in suspended graphene. As the number of experimental reports with the HIM increased, a serious limitation of the helium beam milling in bulk samples has been observed. Since the helium ion interacts with the surface, a small number of surface atoms are sputtered in a very well-controlled area; however, the ions continue to penetrate into the specimen and are implanted at a depth of 100–500 nm (depending on the energy) and remain there. Helium as a noble gas cannot be absorbed into the target specimen, but can be "squeezed" into the space between atoms. At doses above $\sim 10^{16}$ ions/cm^2, however, the pressure of the helium in the target substrate becomes sufficiently large to break the inter-atomic bonds and form helium nanobubbles [45]. It has been reported that a high-power laser pulse can be used in situ during milling to locally heat the target area and alleviate the damage, but crystal defects and surface deformation remain above 1×10^{18} ions/cm^2, which is the required dose to pattern graphene [46]. For reflection-type UV masks, any defects in the atomically precise adsorber stack will lead to a degradation; therefore, hydrogen (which is small and reactive and thus does not cause significant corruption to the target material [14]) or heavier ion species are preferred.

Figure 9a shows a MoSi film on quartz substrate with a single-line etching with a nitrogen-focused ion beam [47]. The cut width of $\sim$ 9 nm is smaller than what can be achieved by gallium, and vertical side walls are achieved for the whole depth. **Figure 9b** shows how the focused nitrogen beam can be used to correct protrusive defects in the MoSi-adsorbing layer. By careful alignment and control of the milling conditions, the repaired edge is not distinguishable from the non-defective edge—an important requirement for mask repair.

N_2 GFIS-FIB was also used for the successful formation of quantum point contacts in high-in-content InGaAs [48], as shown in **Figure 10**. Here, $\sim$ 30-nm wide trenches were carefully aligned to previously wet-etched areas with an inner separation of down to $\sim$ 30 nm, smaller

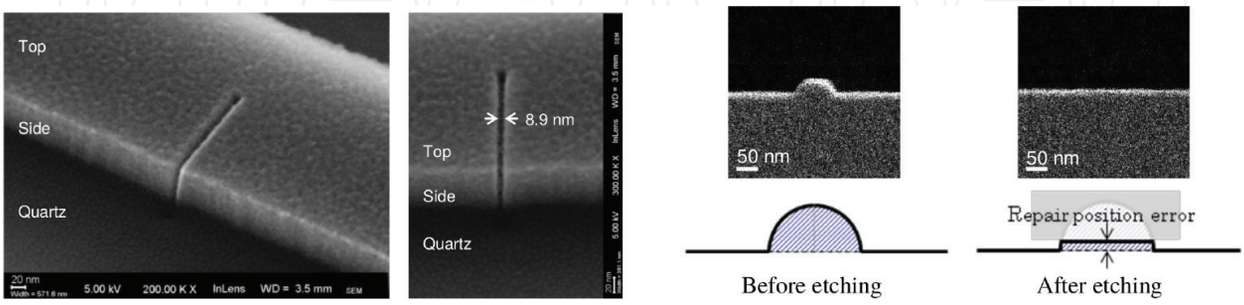

Figure 9. (left) Scanning electron microscopy image of a MoSi film after a one-line etching with the focused nitrogen beam. The width of the deep cut is $\sim$ 9-nm wide. (right) N2IM images showing the removal of protrusive defect in MoSi film on quartz substrate. After removal, the location of the modification is not visible. Reproduced with permission [47].

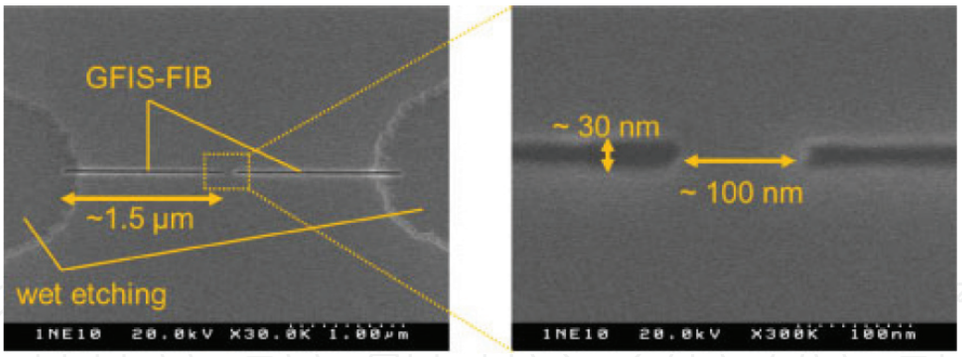

Figure 10. Scanning electron microscopy image of a quantum point contact (QPC) fabricated using N_2 GFIS-FIB. Two horizontal cuts with a width of ~ 30 nm are placed with a separation of ~ 100 nm. Copyright 2014 the Japan Society of Applied Physics [48].

than the size available by electron beam lithography. Half-integer quantized conductance behaviors were observed under magnetic fields, which demonstrates that N_2 GFIS-FIB milling is a promising method to realize quantum devices.

4.3. Other applications

We have shown so far that the N2IM can be used for imaging and milling applications. These can also be performed by helium or neon beams, albeit sacrificing the material contrast discussed in Section 4.1. Nitrogen, however, has a unique effect when implanted into diamond. When a C atom of the diamond lattice is replaced with a nitrogen nearby a vacancy, the so-called nitrogen-vacancy (N-V) center is formed. It has shown to be a scientifically valuable phenomenon as the photoluminescence from a single N-V center can be detected by confocal microscopy [49, 50]. As it turns out, the photoluminescence is affected by magnetic fields [51], electric fields [52], temperature [53], and mechanical stress [54]. Furthermore, N-V centers can be viewed as a basic unit of a quantum computer [55]. To fully exploit these effects, it is necessary to produce N-V centers with nm precision.

To generate N-V centers, either nitrogen implantation followed by annealing is used, or a small amount of nitrogen is added during the chemical vapor deposition of diamond. N-V centers can also be generated by the focused nitrogen ion beam from the GFIS. In this regard, the sub-2-nm beam diameter and variable energy make it a powerful tool. However, some points should be noted about the N-V center generation by ion implantation that needs to be technologically controlled. First, the so-called "conversion efficiency," which signifies the number of N-V centers per implanted nitrogen, is in the single-digit percentage. Therefore, it is not possible to deterministically control the number of N-V centers. Another (smaller) uncertainty is the minute current fluctuation of the GFIS, which means that repeatedly dwelling the beam for a given time will result in different numbers of nitrogen ions and potentially N-V centers; however, this effect is small compared to the conversion efficiency uncertainty. Second, the trajectory of an ion through a solid is subject to a certain randomness. To implant deep N-V centers (which do not disappear through migration to the sample surface during the required postimplantation annealing), a sufficiently large acceleration voltage is required, and the control over the position is lost. As we saw in **Figure 6**, the horizontal distance the ion can travel from the landing point is significant. For nitrogen in a diamond with 12.5 kV, the range

is ∼ 50 nm. A possible solution would be the use of a very low acceleration voltage for the GFIS-FIB nitrogen implantation (thus with an accurate spatial control), followed by an in situ deposition of a diamond capping layer without breaking vacuum. This is certainly an interesting technical challenge.

5. Summary and conclusion

We have given an introduction to the nitrogen ion microscopy (N2IM). Starting with the exciting history, development, and principle of the GFIS, which is at the heart of the recent technological advancement in FIB technology, we have discussed how the molecular nitrogen source gas is different from the atomic source gases. We have reviewed the interaction of nitrogen ions with a silicon sample which shows that nitrogen (N_2) is ionized to N_2^+ and splits within few atomic layers after collision with a sample. The unusual contrast of carbon-based films exposed to a high dose of ion damage in SE images was shown. In terms of machining, nitrogen is a good compromise between helium (high-resolution and low sputter yield) that unfortunately leads to sample swelling at higher doses, and the established gallium (low-resolution and high sputter yield). It was shown how quantum point contacts and photolithographic mask repair is enabled by the nitrogen FIB.

Acknowledgements

This work was supported by the Center of Innovation (COI) program of the Japan Science and Technology Agency and the Grant- in-Aid for Scientific Research No. 25220904, 16K13650, and 16K18090 from the Japan Society for the Promotion of Science (JSPS).

Author details

Marek E. Schmidt*, Masashi Akabori and Hiroshi Mizuta

*Address all correspondence to: schmidtm@jaist.ac.jp

Japan Advanced Institute of Science and Technology, Nomi, Japan

References

[1] Feynman RP. There's plenty of room at the bottom. Engineering and Science. 1960;**23**(5): 22-36

[2] Orloff J, Swanson LW, Utlaut M. Fundamental limits to imaging resolution for focused ion beams. Journal of Vacuum Science & Technology B: Microelectronics and Nanometer Structures Processing, Measurement, and Phenomena. 1996;**14**(6):3759-3763

[3] Hlawacek G, Gölzhäuser A. Helium Ion Microscopy. Cham: Springer; 2016. 536pp

[4] Müller EW. Das Feldionenmikroskop. Zeitschrift für Physik. 1951;**131**(1):136-142

[5] Orloff JH, Swanson LW. Study of a field-ionization source for microprobe applications. Journal of Vacuum Science and Technology. 1975;**12**(6):1209-1213

[6] Orloff J, Swanson LW. Angular intensity of a gas-phase field ionization source. Journal of Applied Physics. 1979;**50**(9):6026-6027

[7] Horiuchi K, Itakura T, Ishikawa H. Emission characteristics and stability of a helium field ion source. Journal of Vacuum Science & Technology B: Microelectronics Processing and Phenomena. 1988;**6**(3):937-940

[8] Tondare VN. Quest for high brightness, monochromatic Noble gas ion sources. Journal of Vacuum Science & Technology A. 2005;**23**(6):1498-1508

[9] Knoblauch A et al. Field Electron emission properties of a Supertip. Journal of Physics D: Applied Physics. 1996;**29**(2):470

[10] Ward B. Spectacular collision of entrepreneurial spirit and a doomed technology transforming the impossible into the helium ion microscope. In: AVS 63rd International Symposium & Exhibition; 2016

[11] Morgan J et al. An introduction to the helium ion microscope. Microscopy Today. 2006; **14**(4):24-31

[12] Ward BW, Notte JA, Economou NP. Helium ion microscope: A new tool for Nanoscale microscopy and metrology. Journal of Vacuum Science & Technology B. 2006;**24**(6):2871-2874

[13] Economou NP, Notte JA, Thompson WB. The history and development of the helium ion microscope. Scanning. 2012;**34**(2):83-89. pmid: 21611954

[14] Aramaki F, Ogawa T, et al. Development of new FIB technology for EUVL mask repair. In: Proceedings of SPIE 7969. Extreme Ultraviolet (EUV) Lithography II. Vol. 7969. San Jose; 2011. pp. 79691C-79691C-7

[15] Bowkett KM, Smith DA. Field-Ion Microscopy. Amsterdam: North-Holland Pub. Co; 1970. 274 pp

[16] Gomer R. Field Emission and Field Ionization. Cambridge: Harvard University Press; 1961. 216 pp

[17] Müller EW, Tsong TT. Field ion microscopy, field ionization and field evaporation. Progress in Surface Science. 1974;**4**:1-139

[18] Orloff J. Field emission ion sources for focused ion beams. In: The Handbook of Surface Imaging and Visualization. Boca Raton: CRC Press; 1995. pp. 165-177

[19] Müller EW, Tsong TT. Field Ion Microscopy: Principles and Applications. New York: American Elsevier Pub. Co; 1969. 336 pp

[20] Schmidt ME, Yasaka A, et al. Nitrogen gas field ion source (GFIS) focused ion beam (FIB) secondary Electron imaging: A first look. Microscopy and Microanalysis. 2017;**23**(4): 758-768

[21] Aramaki F, Kozakai T, Matsuda O, Takaoka O, et al. Photomask repair technology by using gas field ion source. In: Proceedings of SPIE 8441. Photomask and Next-Generation Lithography Mask Technology XIX. Vol. 8441. Yokohama; 2012. pp. 84410D-84410D-6

[22] Kuo H-S et al. Gas field ion source from an Ir/W ⟨111⟩ single-atom tip. Applied Physics Letters. 2008;**92**(6):063106

[23] Wood JA et al. Iridium single atom tips fabricated by field assisted reactive gas etching. Applied Surface Science. 2016;**367**:277-280

[24] Lalanne J-B et al. Note: Electrochemical etching of sharp iridium tip. Review of Scientific Instruments. 2011;**82**(11):116105

[25] Rahman F et al. Field-assisted oxygen etching for sharp field-emission tip. Surface Science. 2008;**602**(12):2128-2134

[26] Lai W-C et al. Xenon gas field ion source from a single-atom tip. Nanotechnology. 2017; **28**(25):255301

[27] McClelland JJ et al. Bright Focused Ion Beam Sources Based on Laser-Cooled Atoms. Applied Physics Reviews. 2016;**3**(1):011302

[28] Viteau M et al. Ion microscopy based on laser-cooled cesium atoms. Ultramicroscopy. 2016;**164**:70-77

[29] Schimmerling W, Vosburgh KG, Todd PW. Interaction of 3.9-Gev nitrogen ions with matter. Science. 1971;**174**(4014):1123-1125. pmid:17779399

[30] Pavlov PV et al. Electron microscopic studies of silicon layers irradiated with high doses of nitrogen ions. Physica Status Solidi. 1976;**36**(1):81-88

[31] Yadav AD, Joshi MC. Formation of thin Si3N4 films by nitrogen ion implantation into silicon. Thin Solid Films. 1979;**59**(3):313-317

[32] Stein SE. 2014 Mass Spectra. In: Linstrom PJ, Mallard WG, editors. NIST Chemistry WebBook. Gaithersburg, MD: NIST Standard Reference Database. 2016. Number 69

[33] Zavilopulo AN, Chipev FF, Shpenik OB. Ionization of nitrogen, oxygen, water, and carbon dioxide molecules by near-threshold Electron impact. Technical Physics. 2005;**50**(4):402-407

[34] Åhlgren EH, Kotakoski J, Krasheninnikov AV. Atomistic simulations of the implantation of low-energy boron and nitrogen ions into graphene. Physical Review B. 2011;**83**(11): 115424

[35] Ziegler JF, Ziegler MD, Biersack JP. SRIM – The stopping and range of ions in matter (2010). Nuclear Instruments and Methods in Physics Research Section B: Beam

Interactions with Materials and Atoms. 2010;**268**(11–12):1818-1823. 19th International Conference on Ion Beam Analysis

[36] Mahady K et al. Monte Carlo simulations of secondary Electron emission due to ion beam milling. Journal of Vacuum Science & Technology B, Nanotechnology and Microelectronics: Materials, Processing, Measurement, and Phenomena. 2017;**35**(4):041805

[37] Ohya K, Ishitani T. Monte Carlo study of secondary Electron emission from SiO2 induced by focused gallium ion beams. Applied Surface Science. Proceedings of the Seventh International Symposium on Atomically Controlled Surfaces, Interfaces and Nanostructures. 2004;**237**(1–4):602-606

[38] Schmidt ME, Yasaka A, et al. Interaction study of nitrogen ion beam with silicon. Journal of Vacuum Science & Technology B. 2017b;**35**(3):03D101

[39] Tan S et al. Gas field ion source and liquid metal ion source charged particle material interaction study for semiconductor Nanomachining applications. Journal of Vacuum Science & Technology B. 2010;**28**(6):C6F15-C6F21

[40] Ramachandra R, Griffin B, Joy D. A model of secondary electron imaging in the helium ion scanning microscope. Ultramicroscopy. 2009;**109**(6):748-757

[41] Goldstein JI et al. Scanning Electron Microscopy and X-Ray Microanalysis: A Text for Biologists, Materials Scientists, and Geologists, 2nd ed. Springer US, 1992

[42] Schmidt ME, Ogawa S, Mizuta H. Contrast differences between nitrogen and helium ion induced secondary electron images beyond instrument effects. MRS Advances. 2018:**3**(10): 505-510

[43] Schmidt ME, Cigang X, et al. Metal-free plasma-enhanced chemical vapor deposition of large area nanocrystalline graphene. Materials Research Express. 2014;**1**(2):025031

[44] Pickard D, Scipioni L. Graphene Nano-Ribbon Patterning in the ORION® PLUS. In: Zeiss application note. 2009

[45] Livengood R et al. Subsurface damage from helium ions as a function of dose, beam energy, and dose rate. Journal of Vacuum Science & Technology B. 2009;**27**(6):3244-3249

[46] Stanford MG et al. In situ mitigation of subsurface and peripheral focused ion beam damage via simultaneous pulsed laser heating. Small. 2016;**12**(13):1779-1787

[47] Aramaki F, Kozakai T, Matsuda O, Yasaka A, et al. Performance of GFIS mask repair system for various mask material. In: Proceedings of SPIE. Photomask Technology 2014. Vol. 9235. Monterey; 2014. pp. 92350F-92350F-8

[48] Akabori M et al. High-in-content InGaAs quantum point contacts fabricated using focused ion beam system equipped with N2 gas field ion source. Japanese Journal of Applied Physics. 2014;**53**(11):118002

[49] Gruber A et al. Scanning confocal optical microscopy and magnetic resonance on single defect centers. Science. 1997;**276**(5321):2012-2014

[50] Iwasaki T et al. Direct nanoscale sensing of the internal electric field in operating semiconductor devices using single Electron spins. ACS Nano. 2017;**11**(2):1238-1245

[51] Balasubramanian G et al. Nanoscale imaging magnetometry with diamond spins under ambient conditions. Nature. 2008;**455**(7213):648-651. pmid: 18833276

[52] Dolde F et al. Electric-field sensing using single diamond spins. Nature Physics. 2011;**7**(6): 459-463

[53] Doherty MW et al. Electronic properties and metrology applications of the diamond NV^- center under pressure. Physical Review Letters. 2014;**112**(4):047601

[54] MacQuarrie ER et al. Mechanical spin control of nitrogen-vacancy centers in diamond. Physical Review Letters. 2013;**111**(22):227602

[55] Wrachtrup J, Jelezko F. Processing quantum information in diamond. Journal of Physics: Condensed Matter. 2006;**18**(21):S807

IntechOpen